Wear, plasticity, and rehybridization in tetrahedral amorphous carbon

Tim Kunze,[1,2,*] Matthias Posselt,[2] Sibylle Gemming,[2] Gotthard Seifert,[1]
Andrew R. Konicek,[3] Robert W. Carpick,[3] Lars Pastewka,[4,5,6] and Michael Moseler[5,6,†]

[1] *Theoretical Chemistry, TU Dresden, D-01062 Dresden, Germany*
[2] *Helmholtz-Zentrum Dresden-Rossendorf, P.O. Box 51 01 19, D-01314 Dresden, Germany*
[3] *Department of Mechanical Engineering and Applied Mechanics, University of Pennsylvania, Philadelphia, PA 19104, USA*
[4] *Department of Physics and Astronomy, Johns Hopkins University, Baltimore, MD 21218, USA*
[5] *Fraunhofer-Institut für Werkstoffmechanik IWM, Wöhlerstraße 11, D-79108 Freiburg, Germany*
[6] *KIT-IWM MicroTribology Center TC, P.O. Box 41 01 03, 76229 Karlsruhe, Germany*

(Dated: December 14, 2012)

Wear in tetrahedral amorphous carbon (ta-C) and diamond is studied by molecular dynamics and near-edge x-ray absorption fine structure (NEXAFS) spectroscopy after self-mated sliding. Both theory and experiment observe the formation of a soft, mainly sp^2 hybridized amorphous carbon (a-C) tribolayer which grows faster for ta-C than for diamond surfaces sliding under otherwise similar conditions. The faster $sp^3 \rightarrow sp^2$ transition in ta-C is explained by easy breaking of prestressed bonds in a nanoscale ta-C region triggered by plasticity in the adjacent a-C while the diamond/a-C transition occurs at an atomically sharp interface.

Tetrahedral amorphous carbon coatings have attracted great scientific and technological attention in recent years because they show low friction in humid environments and have superior resistance to abrasive as well as adhesive wear [1, 2]. These tribological properties make ta-C an outstanding candidate for protective coatings that reduce wear and friction in micro and macro machines [3]. Nevertheless, ta-C coatings abrade under extreme conditions and a mechanistic understanding of the atomic scale wear processes in ta-C is helpful to improve their wear resistance in increasingly demanding applications [4, 5].

Wear in ductile metals [6] is typically linked to microfatigue through fracture and plasticity [7]. For brittle ceramics, wear progresses through brittle micro-fracture, although plasticity is also observed [8]. Continuous mild wear in amorphous films is understood to a much lesser extent, but it is well known that bulk amorphous metals fail through shear bands which are localized plastic events [9]. We propose here that the sliding interface between two amorphous surfaces can be regarded as a shear band since it necessarily exhibits shear localization.

Shear banding is accompanied by a change in local order of the material [10, 11]. Mesoscopic models of plasticity rely on an order parameter field $\phi(\vec{r})$ that characterizes the degree of local order. Examples are the effective temperature in shear transformation zone theory [12, 13] or the liquid-like material concentration in amorphous silicon [14]. A typical evolution equation then couples the order parameter field $\phi(\vec{r})$ to the locally integrated amount of local plastic strain γ [15]:

$$d\phi = f(\phi)d\gamma \tag{1}$$

We here investigate such plastic processes for ta-C. The tribointerface is naturally weak and we find a shear-band like localization of the strain in that region. In our molecular dynamics (MD) simulations, an a-C phase with low sp^3 content forms between ta-C/ta-C tribo partners. Interestingly, the a-C formation rate in the ta-C/a-C/ta-C system exceeds the amorphisation rate in diamond/diamond tribo couples [16]. This is in excellent qualitative agreement with our NEXAFS analysis that suggests an enhanced a-C formation for the ta-C case compared to ultrananocrystalline diamond (UNCD) [17, 18]. Motivated by these observations, we choose the local hybridization, in particular the fraction of sp^3 coordinated carbon atoms as our order parameter. Our simulations show that a local coupling as given by Eq. (1) must be invalid for the particular case of ta-C. In particular, rehybridization *precedes* plastic events and the material needs to be weakened before it yields. This is possible because a large fraction of bonds in ta-C are severely prestressed and require only minute perturbation to break. We contrast this behavior with diamond-diamond tribocouples that show similar shear localization, but where the diamond to a-C transformation is confined to a region of low but finite shear rate [16].

For our atomistic simulations, we prepare two independent ta-C films by a liquid carbon quench from two opposing diamond surfaces. This results in a stack of two 2.9 nm x 3.0 nm x 5.5 nm ta-C films with roughly 70 % sp^3 concentration. The ta-C film structure agrees well with reported data on realistically grown films as well as DFT calculations [19–21]. Periodic boundary conditions are applied in lateral directions. In our simulations, we assume that any surface termination will eventually dissociate [22] and the two sliding counterfaces weld. Hence, we cut the two films to expose a bare ta-C surface for each. We pair two incommensurate surfaces to form a sliding system with a weak plane where sliding initiates. This sliding setup is similar to previous work on self-mated ta-C surfaces [23]. The top and bottom section of the sliding system is subdivided into three layers as

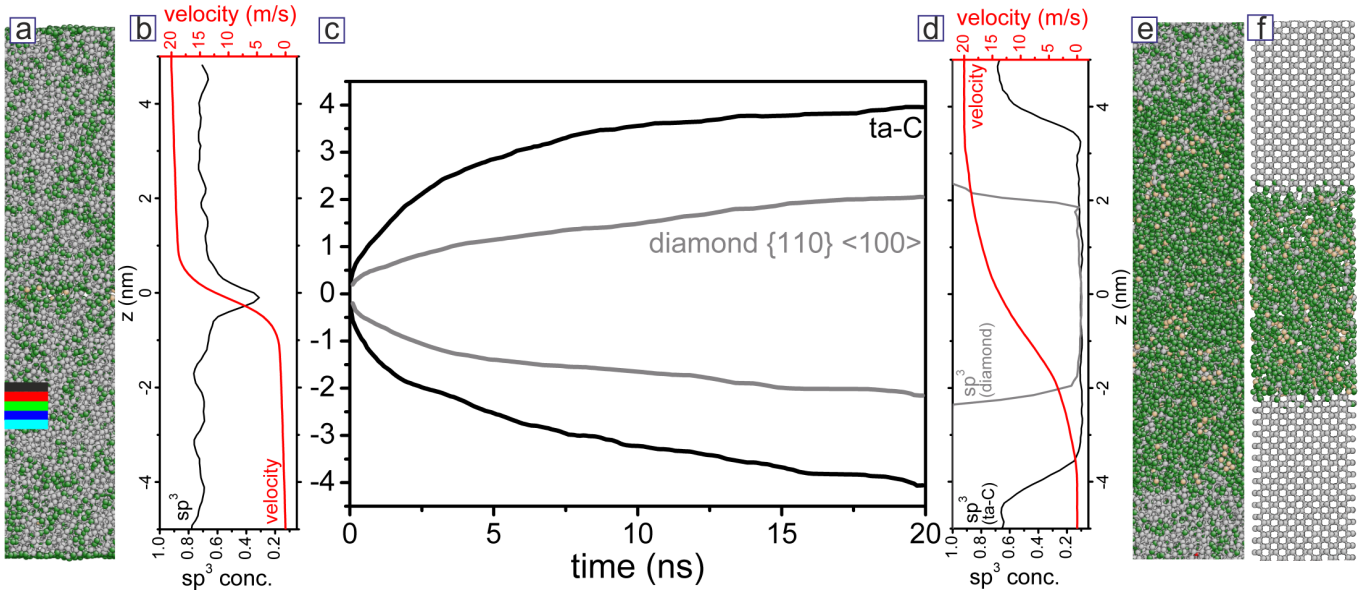

FIG. 1. (Color) (**a**) snapshot of the ta-C/ta-C tribosystem after 0.1 ns of sliding. Atoms are color-coded according to their atomic coordination: white → 4-fold (sp^3), green → 3-fold (sp^2), yellow → 2-fold (sp^1). The colored bars define layers that were used for further analyses in Fig. 3.(**b**) sp^3 concentration (black curve) and velocity profile (red curve) across the ta-C/ta-C tribo couple. (**c**) Evolution of the upper and lower boundary of the a-C tribofilm formed between two ta-C surfaces (black curve) compared to a corresponding film formed between two diamond {110} surfaces rubbed in ⟨001⟩ direction (gray curve). (**d**) sp^3 concentration (black curve for ta-C and gray curve for diamond) and velocity profile of the ta-C system (red curve) after 20 ns of sliding. (**e**) and (**f**) snapshot of the ta-C/ta-C and diamond/diamond tribo systems after 20 ns sliding.

described in Ref. [24]. The atomic positions of the outermost 0.4 nm layer is fixed and a T=300 K Langevin thermostat is applied to an adjacent 0.6 nm wide layer. The motion of the remaining atoms between the two thermostated layers of the two ta-C films is calculated from Newton's equations. We employ the second generation reactive empirical bond-order potential (REBO2) [25] that is supplemented by an improved nearest-neighbor cutoff scheme [21]. Such a construction is mandatory for a reasonable description of bond-breaking and forming processes during friction. A load of 10 GPa is then applied to the fixed atoms of the upper ta-C film. The construction of our barostat compensates for the finite-size of the simulated system [24]. A sliding velocity of $v_S = 20$ m s^{-1} is instantly applied to the upper fixed layer. By construction, the initial ta-C/ta-C tribo couple consist of two 70% sp^3 ta-C films separated by a sub-nanometer layer of a-C. Figure 1a shows a snapshot of the ta-C/ta-C tribosystem after 0.1 ns of sliding.

The a-C layer is clearly associated with a drop in the sp^3 concentration profile in Fig. 1b and accommodates all the sliding induced shear (see velocity profile in Fig. 1b). The region near the sliding interface undergoes a phase transition from sp^3 to sp^2 hybridized carbon that leads to the formation of additional a-C tribomaterial between the ta-C regions. This is consistent with earlier simulation on the initial stage of sliding at 100 m s^{-1} [23]. The width of the a-C interlayer grows with increasing sliding distance (black curve in Fig. 1c) and exhibits a square-root-like dependence in time similar to the a-C that forms between sliding diamond surfaces [16]. For reference, the gray curve in Fig. 1c shows the pairing of the softest diamond tribo couple that exhibit a significantly slower growth of the a-C interlayer.

After 20 ns of sliding ta-C and diamond, a rather homogeneous distribution of 70 - 80 % sp^2 carbon with equal sp^1 and sp^3 residues can be detected within the a-C tribolayers. This is illustrated in the sp^3 concentration profiles in Fig. 1d and the atomic structure of the ta-C system in Fig. 1e. Furthermore, the $sp^3 \rightarrow sp^2$ transition region spreads over a 1 nm wide layer in contrast to the sharp diamond/a-C interface in the diamond simulations. The corresponding ta-C (black) and diamond (gray) sp^3 profiles in Fig. 1d clearly show the extent of this transition region where the distinct diamond/a-C interface also clearly appears in the atomic structure in Fig. 1f. Interestingly, the ta-C/a-C $sp^3 \rightarrow sp^2$ transition region is not taking part in the shear process. All tribo-induced plasticity is restricted to the soft, high-sp^2 region as can be seen by comparing the velocity profile (red) in Fig. 1d to the hybridization profile (black).

Wear experiments on ta-C and diamond support our theoretical results. We analyzed the NEXAFS spectra from Ref. [17] in order to estimate the amount of a-C that is formed in ta-C/ta-C and diamond/diamond pairings. In that reference, the diamond material is UNCD, which

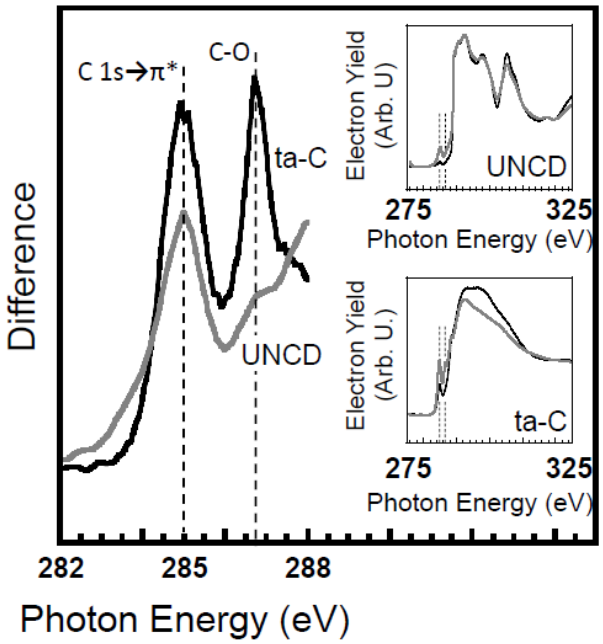

FIG. 2. Difference in representative NEXAFS total electron yield spectra between worn and unworn regions of carbon-based films. Black curve: difference between a spectrum taken from a heavily worn (high load, low relative humidity) ta-C wear track and a spectrum from unworn ta-C. Gray curve: difference between a spectrum taken from heavily worn UNCD and unworn UNCD. The upper inset shows the worn (gray) UNCD spectrum and the unworn (black) UNCD spectrum. The lower inset shows the worn (gray) ta-C spectrum and the unworn (black) ta-C spectrum.

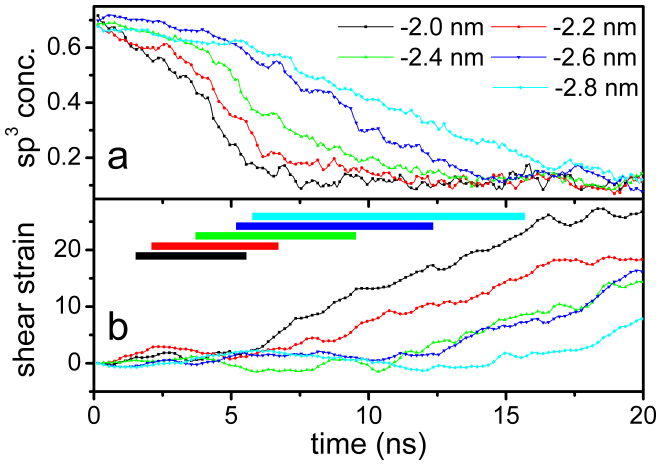

FIG. 3. (Color) Evolution of sp^3 concentration (**a**) and shear strain (**b**) in the stack of 5 layers as described in the text. The color code distinguishes the height of the layers (see also bars in Fig. 1a). The colored bars in (**b**) denote the main rehybridization region (transition region between 60 % and 20 % sp^3 concentration) of the respective layers.

initially has ∼95% sp^3-bonded carbon and where the sp^2-bonded carbon is exclusively found at grain boundaries or at the surface. Fig. 2 shows the difference between spectra taken from the worn and unworn ta-C and UNCD surfaces. The increase in the magnitude of the C 1s → π^* peak at 285 eV was 43% greater for ta-C than for UNCD, demonstrating a significantly higher conversion rate from sp^3- to sp^2-bonded carbon. This is the case even though the normal load for the ta-C test was half that for the UNCD test (all other conditions were the same, as discussed in Ref. [17]). In addition, there is a significant increase in CO bonds as seen in the ta-C difference spectrum, which is further evidence that a large number of surface bonds were broken, as these interact further with oxygen from the environment.

To further study the mechanism that underlies the ta-C/a-C phase transformation, we analyze the evolution of the average sp^3 concentration in a stack of five layers of Δz=0.2 nm thickness within the lower ta-C film. These layers are indicated by the colored bars in Fig. 1a. They are located between z=-1.9 nm and z=-2.9 nm below the initial sliding plane. In the five layers, the initial sp^3 concentration is about 70% and during 20 ns of sliding this concentration decreases to about 10 % (Fig. 3a). The onset of this phase transformation depends on the height of the layers within the lower ta-C film. Horizontal bars in Fig. 3b mark the time interval in which each layer's sp^3 concentration drops from 60% to 20% and show clearly that the more distant layers transform later.

Next, we consider the evolution of shear strain $\gamma(z,t)$ in a layer at height z which is determined from the shear rate $\frac{\partial v(z,t)}{\partial z}$ by $\gamma(z,t) = \int_0^t dt' \frac{\partial v(z,t')}{\partial z}$. The shear rate within a layer is calculated as a finite difference of the velocities $v(z \pm \Delta z/4, t)$ of two sub-layers of height $\Delta z/2$=0.1 nm. Fig. 3b depicts the evolution of the local strain $\gamma(z,t)$ for the five individual layers. Each layer starts with fluctations around zero strain followed by a clear transition to a linear increase in strain. Remarkably, this onset of plastic deformation takes place *after* the layer has transformed to an a-C. Note, that the end of the colored bars that show the transformation region in Fig. 3b coincide with the onset of plastic strain. Thus, any mechanism that connects the $sp^3 \rightarrow sp^2$ transformation to local plasticity can be ruled out.

On the other hand, it becomes evident from Figs. 3a and 3b that the ta-C/a-C phase change takes place close to the strained part of the tribosystem. The "black" layer in Fig. 3b starts to yield at roughly 5 ns and at the same time the sp^3 concentration of the 0.6 nm deeper lying "blue" layer begins to drop. This suggests that rehybridization must be driven by fluctuations in stress that propagate from the continuously sheared a-C into the stationary ta-C bulk. In order to test this hypothesis we investigate the influence of structural rearrangements at the ta-C/a-C interface on deeper lying ta-C layers with an auxiliary simulation. A 5.8 nm thick ta-C film with 70% sp^3 concentration and lateral dimensions 2.6 nm × 2.6 nm

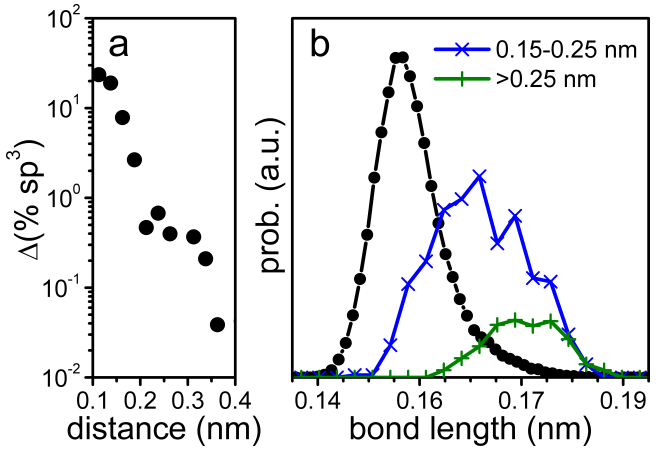

FIG. 4. (Color) **a** Average change of the sp^3 hybridization depending on the distance from the L/U interface (according to the auxiliary calculations as described in the text). **b** Distribution of bond length of all bonds that get broken by the shift in the auxiliary simulations *before* perturbing the system. Black curve: all bonds; blue curve: 0.15 to 0.25 nm away from the perturbation; and green curve more than 0.25 nm away from the perturbation.

is split equally into an upper (U) and lower (L) part. The U part is then rigidly shifted by a distance Δx in lateral direction. In this way, the force network at the L/U interface is drastically changed, mimicking the strong plastic events in the a-C of our previous tribosimulation. Finally, the whole system is relaxed [26] and the induced rehybridization is analyzed. Fig. 4a depicts the change of the sp^3 content in the vicinity of the L/U interface. This data is obtained as an average over 10 different Δx in 20 independent L/U samples. Besides the expected strong drop of sp^3 near the L/U interface (less than 0.2 nm away from the perturbation), we observe also rehybridization events that are almost 0.4 nm away from the L/U interface. This finding clearly indicates that the continuous change of the force network at the ta-C/a-C interface affects the structural integrity of the deeper layers in ta-C and promotes the rehybridization.

The resistivity to these force fluctuations can be determined by investigating the bond length distribution in the ta-C film *prior* to the rigid shift of U. Any event that promotes an sp^3 carbon atom into an sp^2 state requires the breaking of a bond. The black curve in Fig. 4b displays the distribution of bond lengths between all atom pairs with at least one sp^3 hybridized atom (i.e. sp^2-sp^3 and sp^3-sp^3 bonds). The same distribution function can be recorded for the subset of these bonds that will be broken *after* the rigid U shift. Fig. 4b shows these distributions for bonds that were closer (blue) and further away (green) from the L/U interface. It is apparent that the broken sp^2-sp^3 and sp^3-sp^3 bonds were already elongated and thus weakened *before* the rigid U shift. This suggests that sp^2-sp^3 and sp^3-sp^3 bonds with tensile prestress will break first when exposed to force fluctuations from the changed L/U interface. All sp^2-sp^2 bonds stayed intact during this procedure.

Within this picture it is now easy to understand why the a-C formation rate is smaller in diamond than in ta-C. Since a-Cs that formed in the ta-C/ta-C and diamond/diamond simulations are identical in terms of its hybridization mixture (Fig. 1d), the force fluctuations that are injected into ta-C and diamond are of the same order of magnitude. Bulk diamond lacks the structural inhomogeneities that are characteristic for glassy materials. Its bulk bonds can only be prestressed by an external homogeneous shear stress τ (note that for $\tau = 10$ GPa the related bond length elongation is less than 0.01 nm). Thus, only bonds at the diamond/a-C interface are weak enough to break, which leads to an atomically sharp diamond/a-C interface and a correspondingly small amorphization rate. Conversely, a significant fraction of the bulk ta-C bonds have tensile prestress (many of them are elongated by more than 0.02 nm) and therefore are easier to break, consequently leading to a higher a-C formation rate and a $sp^3 \rightarrow sp^2$ transition region of finite size.

Our results show that localized plastic events transform the surrounding material to a weaker state even in the presence of highly compressive external stresses. The non-local character of this process is in remarkable contrast to current models for plasticity in amorphous materials, but solves the chicken or egg problem of whether plasticity causes changes in the order parameter field or vice-versa. While ta-C could be a special case, it is likely that other materials exhibit similar non-local behavior. The study of this particular phenomenon requires gradients in the order parameter field. Here, those were initially generated through the pairing of two disjunct ta-C surfaces, but most computational studies of plasticity start from a homogeneous initial configuration in which it is difficult to disentangle non-local effects.

With regards to the wear resistance of ta-C, the $sp^3 \rightarrow sp^2$ transformation dissipates energy and prevents catastrophic failure through brittle fracture such as observed on the hardest (111) surface of diamond [16, 27]. Hence while in bulk glasses shear localization is responsible for the failure of the material [9], here it is the source of the toughness under tribological loading. The weak character of the a-C tribointerface eventually allows easy "failure" upon separation of contacting asperities. The exposed surface is a soft layer on a hard substrate that would be eventually removed through abrasive or chemical processes [28–30].

We thank M.L. Falk, P. Gumbsch, M.O. Robbins and K.M. Salerno for useful discussion. T.K. and G.S. acknowledge funding by the European Center for Emerging Materials and Processes (ECEMP), financed by the European Union and the Free State of Saxony (project no. 13857/2379). R.W.C. and A.K. acknowledge support

from the Air Force Office of Scientific Research under Contract No. FA2386-11-1-4105 AOARD, and from the UPenn MRSEC Program of the National Science Foundation under award No. DMR11-20901. We acknowledge W.G. Sawyer for tribological measurements, A.V. Sumant for providing UNCD films, and T.A. Friedmann for providing ta-C films. L.P. acknowledges funding from the European Commission (Marie-Curie IOF 272619). Computations were carried out at the Jülich Supercomputing Center.

* t.kunze@hzdr.de
† michael.moseler@iwm.fraunhofer.de

[1] J. Robertson, Mater. Sci. Eng. R. **37**, 129 (2002).
[2] A. Erdemir and C. Donnet, J. Phys. D: Appl. Phys. **39**, R311 (2006).
[3] S. Cho, I. Chasiotis, T. A. Friedmann, and J. P. Sullivan, J. Micromech. Microeng. **15**, 728 (2005).
[4] J. Hershberger, O. Öztürk, O. O. Ajayi, J. B. Woodford, A. Erdemir, R. A. Erck, and G. R. Fenske, Surf. Coat. Technol. **179**, 237 (2004).
[5] C. P. O. Treutler, Surf. Coat. Technol. **200**, 1969 (2005).
[6] J. F. Archard and W. Hirst, Proc. R. Soc. Lond. A **236**, 397 (1956).
[7] A. Kapoor and K. L. Johnson, Proc. R. Soc. Lond. A **445**, 367 (1994).
[8] H. Kong and M. F. Ashby, Acta Metall. Mater. **40**, 2907 (1992).
[9] C. A. Pampillo and H. S. Chen, Mater. Sci. Eng. **13**, 181 (1974).
[10] Y. Shi and M. L. Falk, Phys. Rev. Lett. **95**, 095502 (2005).
[11] M. Widom, K. J. Strandburg, and R. H. Swendsen, Phys. Rev. Lett. **58**, 706 (1987).
[12] M. L. Falk and J. S. Langer, Annu. Rev. Condens. Matter Phys. **2**, 353 (2011).
[13] M. L. Falk and J. S. Langer, Phys. Rev. E **57**, 7192 (1998).
[14] M. J. Demkowicz and A. S. Argon, Phys. Rev. Lett. **93**, 025505 (2004).
[15] A. S. Argon and M. J. Demkowicz, Metall. Mater. Trans. A **39A**, 1762 (2008).
[16] L. Pastewka, S. Moser, P. Gumbsch, and M. Moseler, Nature Mater. **10**, 34 (2011).
[17] A. R. Konicek, D. S. Grierson, A. V. Sumant, T. A. Friedmann, J. P. Sullivan, P. U. P. A. Gilbert, W. G. Sawyer, and R. W. Carpick, Phys. Rev. B **85**, 155448 (2012).
[18] A. R. Konicek, D. S. Grierson, P. U. P. A. Gilbert, W. G. Sawyer, A. V. Sumant, and R. W. Carpick, Phys. Rev. Lett. **100**, 235502 (2008).
[19] H. U. Jäger and K. Albe, J. Appl. Phys. **88**, 1129 (2000).
[20] C. W. Chen and J. Robertson, Diamond Relat. Mater. **15**, 936 (2006).
[21] L. Pastewka, P. Pou, R. Pérez, P. Gumbsch, and M. Moseler, Phys. Rev. B **78**, 161402(R) (2008).
[22] J. A. Harrison and D. W. Brenner, J. Am. Chem. Soc. **116**, 10399 (1994).
[23] J. D. Schall, G. Gao, and J. A. Harrison, J. Phys. Chem. C **114**, 5321 (2010).
[24] L. Pastewka, S. Moser, and M. Moseler, Tribol. Lett. **39**, 49 (2010).
[25] D. W. Brenner, O. A. Shenderova, J. A. Harrison, S. J. Stuart, B. Ni, and S. B. Sinnott, J. Phys.: Condens. Matter **14**, 783 (2002).
[26] E. Bitzek, P. Koskinen, F. Gähler, M. Moseler, and P. Gumbsch, Phys. Rev. Lett. **97**, 170201 (2006).
[27] J. R. Hird and J. E. Field, Proc. R. Soc. Lond. A **460**, 3547 (2004).
[28] G. Moras, L. Pastewka, M. Walter, J. Schnagl, P. Gumbsch, and M. Moseler, J. Phys. Chem. C **115**, 24653 (2011).
[29] G. Moras, L. Pastewka, P. Gumbsch, and M. Moseler, Tribol. Lett. **44**, 355 (2011).
[30] M. Krishnan, J. W. Nalaskowski, and L. M. Cook, Chem. Rev. **110**, 178 (2010).